Natural and synthetic metal oxalates-a topology approach

CrystEngComm

PAPER

View Article Online
View Journal | View Issue

Cite this: CrystEngComm, 2019, 21, 6156

Natural and synthetic metal oxalates – a topology approach†

Cyrielle L. F. Dazem,[a] Francoise M. Amombo Noa,[b] Justin Nenwa[a] and Lars Öhrström *[b]

Oxalates are found in minerals and in biology, are made in the laboratory, and are used on an industrial scale. They form coordination polymers and hydrogen bonded networks that often can be analysed using network topology. In this survey of known naturally occurring oxalates we note weddellite, $[Ca(C_2O_4)]\cdot xH_2O$, that seems to be the first known naturally occurring metal–organic framework, forming the four-connected **crb**-net (zeolite CRB). The natural oxalates are typically 3D, 2D or 1D coordination polymers, with extensive hydrogen bonding in the latter cases. For example, humboldtine and lindbergite form the new 3- and 8-connected net **hum** by combining the 1D structure with strong hydrogen bonds. Tris-oxalates rarely occur in nature but stepanovite, $[Mg(H_2O)_6][Na[Fe(ox)_3]]\cdot 3H_2O$, is an exception and forms **hcb**-nets (honeycomb 2D layers) with the hexaaqua ions sealing any potential voids. Synthetic tris-oxalates on the other hand are well explored and normally form 2D **hcb**-nets or 3D chiral three-connected **srs**-nets. Theoretically a few other topologies should also be possible, and it was found that [Mn((*R*)-salmen)(CH_3OH)(CH_3CN)][$MnCr(ox)_3$]·0.5CH_3OH·1.25CH_3CN forms the achiral three-connected **lig**-net, [Fe(2,6-bis(pyrazol-3-yl)pyridine)$_2$][$MnCr(ox)_3$]·2,6-bis(pyrazol-3-yl)pyridine·CH_3OH forms the likewise achiral **nod**-net and [Cu(trans[14]dien)][$KCr(ox)_3$] the **ths**-net. A new binodal 3-connected net **noa** (with the derived 3c-,4c- new net **mys**) was found in $[Fe^{II}(tren(imid)_3)]_2[Mn_{2.5}(CH_3OH)_3Cr_3(ox)_9]\cdot(CH_3OH)_{4.75}\cdot(H_2O)_4$. The more complex $[Fe(tren(imid)_3)]_2[Mn_{2.5}(CH_3OH)_3Cr_3(ox)_9]$ forms a new three-nodal 3-connected **daz**-net.

Received 30th July 2019,
Accepted 13th September 2019

DOI: 10.1039/c9ce01187k

rsc.li/crystengcomm

1. Introduction

Oxalic acid and oxalates date far back in human history, both found as a tasty part of numerous plants, and in painful and dangerous kidney and bladder stones. In industry, they are used in the separation of various metals, and other practical examples employing the ubiquitous $C_2O_4^{2-}$ unit are in artistic chemical photography processes and the anticancer drug oxaliplatin (trade name Eloxatin).[1] But oxalates are also very much present in today's cutting edge science.[2–7] Recently, for example, MOFs from tetrakis oxalates with zeolite topologies have been prepared.[3]

Tri-potassium trioxalato-rhodium monohydrate was the focus of the first diffraction study of oxalates in 1927 (ZZZVZK)[8] followed by beryllium oxalate trihydrate in 1928 (ZZZQZK), and today the Cambridge Crystallographic Data Centre has collected over 6000 oxalate entries into the CSD.

Due to the possibility of the oxalate ion forming bridging chelates in two or more directions, and its many hydrogen bond accepting sites, oxalate compounds often form networks. The topological analysis of such networks has its origins in the work of Alexander Wells starting in the 1950s,[9,10] gaining popularity by the analysis of coordination polymers and metal–organic frameworks (MOFs) in the 1990s and onwards.[11–13]

Here, we report how well metal compounds with small oxalate ions (ox) lend themselves to such topological analysis. We will show the importance of network topologies in both the synthesis of new oxalate compounds and in the communication and understanding of known oxalates, both natural and synthetic.[14]

We have investigated two cases, first the tris-oxalates, $[M'M(ox)_3]$, forming three-connected networks. These are known to produce 2D **hcb**-nets (honeycomb nets, Fig. 1 left) or the 3D chiral **srs**-nets (or (10,3)-a, Fig. 1 right), but geometrical considerations suggest that also a number of other 3-connected topologies should be conceivable, even though the **srs**-net appears to be the perfect fit for enantiomerically pure tris-oxalates.[13,15]

We do not consider the four-connecting tetrakis-oxalates here if they are not naturally occurring, as these have been discussed elsewhere.[3,16]

[a] Inorganic Chemistry Department, Faculty of Science, University of Yaoundé I, PO. Box 812, Yaoundé, Cameroon. E-mail: cyrielle_leyla@yahoo.fr, jnenwa@yahoo.fr
[b] Chemistry and Biochemistry, Dept. of Chemistry and Chemical Engineering, Chalmers University of Technology, SE-41296 Göteborg, Sweden. E-mail: mystere@chalmers.se, ohrstrom@chalmers.se

† Electronic supplementary information (ESI) available. See DOI: 10.1039/c9ce01187k

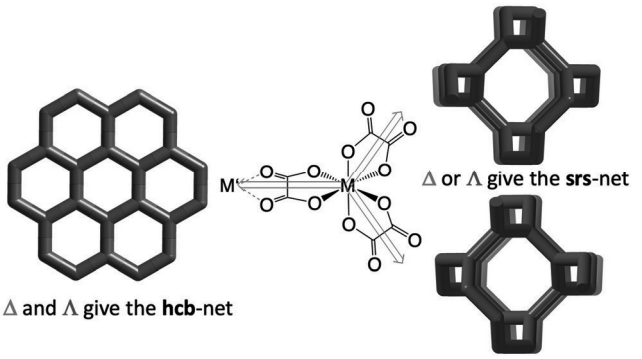

Fig. 1 Tris-oxalates, $[M'M(ox)_3]$, form three-connected networks. These are known to produce 3D chiral **srs**-nets (right) with only one enantiomer and 2D **hcb**-nets (left) when both enantiomers are present.

Secondly, we consider the natural oxalates, recently reviewed by Piro and Baran.[17] Through the 2D tris-oxalate **hcb**-nets there is some overlap with the first group,[18] and the rare Siberian mineral stepanovite had its 15 minutes of fame a few years ago[19,20] when the structures were, unexpectedly, found to resemble "well-established magnetic and proton-conducting metal oxalate MOFs".[21]

2. Experimental

2.1 Materials and methods

2.1.1 Searching the Cambridge Structural Database (CSD). The CSD 5.40 (September 2019) was used. In all runs the Conquest software (version 2.0.2 or 2.0.3) was used. To compute bridging tris-oxalates, an $[M_3[M(ox)_3]]$ entity was used as a query, and to exclude the tetrakis-oxalates and only include extended networks, the central M was restricted to a maximum of 7 bonding atoms and at least one M–O bond was specified as polymeric.

2.1.2 Computational details. The network topologies discussed in this article were obtained using the freeware programs ToposPro[22] and Systre[23] operating on the original crystallographic information files for the compounds in question, or on files derived from these. Throughout we discuss the topologies using three-letter symbols in the web-based and free Reticular Chemistry Structural Resource database, RCSR,[24] as encouraged by IUPAC.[25]

3. Results and discussion

3.1 Tris-oxalates, $[M'M(ox)_3]^{x-}$

The Cambridge Structural Database in total contains 682 entries with a minimum of three bridging oxalates (15 added to the latest 5.40 tri-annual update), and at least 301 of these are tris-oxalate networks either with M = M′ or with different M and M′. A recent survey of **srs**-nets (Fig. 1) lists 91 tris-oxalates having the **srs**-network topology,[26] and as not all of the remaining ones form the 2D **hcb**-net (Fig. 1), we wondered about these network topologies. Is there one particular topology that is the second "choice" or are there many possibilities? And are they all chiral as the **srs**-net?

In Table 1, we have collected the tris-oxalates from the CSD that form neither the **srs** nor **hcb**-net.

3.1.1 The lig-net. The **lig**-net (from LiGe, a Zintl phase with a three-connected Ge network) was identified by Blatov *et al.* in the coordination polymer $[CdCl(tpht)(PPh_3Bz)]$, YINPEQ, where it is doubly interpenetrated.[12] It was also briefly discussed as a rod-packing by Rosi *et al.*[27] We found it in the metal-oxalate network in BEWVEG, $[Mn((S)\text{-salmen})(CH_3OH)_2][MnCr(ox)_3](CH_2Cl_2)_{0.375}(CH_3OH)_{0.375}(H_2O)_{0.125}$,[28] see Fig. 2.

Compared to the nets discussed by Öhrström & Larsson that were all formed from 10-gons as the shortest rings between nodes, the **lig**-net also forms 8-rings (point symbol $8^2{\cdot}10$ and vertex symbol $8{\cdot}8{\cdot}10_3$ (ref.15)). This and other three-connected nets are discussed in detail in ref. 13.

3.1.2 The nod-net. The **nod**-net also forms 8-rings, but is a binodal net with the point symbol[29] $8^2{\cdot}10{\cdot}8^2{\cdot}10$ and the vertex symbol[29] $8{\cdot}8{\cdot}10_3$ $8{\cdot}8{\cdot}10_3$. The metal-oxalate network in GURPIT, $[Fe(sal_2\text{-trien})][MnCr(ox)_3]{\cdot}CH_3OH$,[30] forms the **nod**-net, see Fig. 3.

3.1.3 The ths-net. The **ths**-net (from $ThSi_2$, also known as the 10,3-b net) is similar to the **srs**-net as it is also a 10,3-net, meaning that all the shortest rings are 10-gons. Its point symbol is 10^3 just as the **srs**, but the vertex symbols differ; $10_5{\cdot}10_5{\cdot}10_5$ for **srs** *versus* $10_2{\cdot}10_4{\cdot}10_4$ for **ths** (meaning that the number of different 10-gons forming the shortest circuits differ). A further difference is that **ths** is achiral and does not have the characteristic four-fold helices of **srs**, **lig**, **nod**, and some other 3-connected nets.

We found this net in for example $[Cu(trans[14]dien)][KCr(ox)_3]$,[31] where trans[14]dien is 5,7,7,12,14,14-hexamethyl-1,4,8,11-tetraazacyclotetradeca-4,11-diene. In Fig. 4, it is shown (right) together with the ideal version of the **ths**-net (left).

3.1.4 The noa-net. While the preceding nets have all been described and found in various compounds (occurrence can be checked with ToposPro) we were surprised to find a new two-nodal three-connected net **noa** in RUGKIP $(o\text{-}FAni^+)_2(DCH[18]crown\text{-}6)_2[Mn(CH_3OH)\ Cr(oxalate)_3][MnCr(oxalate)_3](CH_3OH)$.[32] This new net has point symbols $4{\cdot}8{\cdot}10$ and $8{\cdot}10^2$ and again we see the characteristic four-fold helices in a racemic set-up, but this time connected by four rings. This enforces 90° angles in the network, and this is achieved by one of the Mn ions having one mono-coordinated oxalate ion and a methanol molecule completing the octahedron. The ideal net and the network in RUGKIP are presented in Fig. 5.

It has not escaped us that the **noa**-net is an augmented form of a three- and four-connected net with the four connected nodes in the centre of the squares. Somewhat surprisingly this is not the known **jph**-net[16] but yet another new topology, **mys**, with point symbols $6{\cdot}8^2$ and $6^2{\cdot}8^2{\cdot}10^2$. They differ again, just as **lig** and **nod**, in the arrangement of the four-fold helices of opposite chirality, see ESI† Fig. S1.

3.1.5 The daz-net. To finish off this section we want to comment on a more complicated structure. $[Fe^{II}$(tren-

Table 1 Tris-oxalates $[M'M(ox)_3]^{X-}$ from the CSD that form neither the **srs** nor **hcb**-net

M′M	Cation	CSD	Net
Mn(II) Cr(III)	$[Mn((S)\text{-salmen})(CH_3OH)_2]^+$	BEWVEG	**lig**
Mn(II) Cr(III)	$[Mn((R)\text{-salmen})(CH_3OH)_2]^+$	BEWVOQ	**lig**
Mn(II) Cr(III)	$[Fe(imid_2\text{-trien})]^{2+}$	VINHOR	**lig**
Mn(II) Cr(III)	$[Fe(tren(6\text{-Me-py})_3)]^{2+}$	VINHIL	**lig**
Mn(II) Cr(III)	$[Fe(2,6\text{-bis(pyrazol-3-yl)pyridine})_2]^{2+a}$	EDATOT	**nod**
Mn(II) Cr(III)	$[Fe(sal_2\text{-trien})]^{3+}$	GURPIT	**nod**
Mn(II) Cr(III)	$[In(sal_2\text{-trien})]^{3+}$	GURPOZ	**nod**
Mn(II) Cr(III)	$[In(sal_2\text{-trien})]^{3+}$	GURPUF	**nod**
Mn(II) Cr(III)	$[Fe(5\text{-}CH_3Osal_2\text{-trien})]^{3+}$	PUWZOX	**nod**
Mn(II) Cr(III)	$[Mn(salen)(H_2O)]_2^{2+}$	PIQFIG	**nod**
Mn(II) Cr(III)	$(H_2PPD^+)(benzo[18]crown\text{-}6)_2$	RUGKEL	**nod**
K(I) Cr(III)	$[Cu(trans[14]dien)]^{2+}$	QIYXIF	**ths**
Cu(II)	$HN(Et)_2(CH_2CH_2OH)^+$	KIRFIA	**ths**
Cu(II)	$HN(Et)_3^+$	KEDJAG	**ths**
Mn(II) Cr(III)	$[Fe(tren(imid)_3)]_2^{2+}$	VINHEH	**daz**[b]
Mn(II) Cr(III)	$(o\text{-}FAni^+)_2(DCH[18]crown\text{-}6)_2$	RUGKIP	**noa**[b]

[a] Severely disordered. [b] New topologies.

$(imid)_3)]_2[Mn_{2.5}(CH_3OH)_3Cr_3(ox)_9]\cdot(CH_3OH)_{4.75}\cdot(H_2O)_4$[33] has both bridging and terminal oxalates, as well as a *bis* oxalate entity with terminating methanol ligands. This gives a total of six symmetry independent coordination entities in the structure, but only three of these are nodes in the network shown in Fig. 6.

The resulting network topology is tri-nodal and chiral, but would be of limited interest to the crystal engineering community if it was not for its clear relationship to the nets already discussed and to other similar nets in the RCSR. The point symbols are 8^3, 8^3, and $8{\cdot}10^2$ and the Topos topological type is 3,3,3 T12.

As can be seen in Fig. 6 (left), the ideal **daz**-net resembles the **srs**-net, only with a zigzag motif added between helices along the *z*-axis. It is also related to the likewise chiral binodal **noj**-net that essentially is an **srs**-net with the zigzag motif inserted between all helices.

It is currently not known if there are similar versions of the achiral **lig** and **nod** nets.

We note, however, that the analysis of the structure using the **daz**-net greatly simplifies the task and renders "a very irregular 3D oxalate network"[33] into a reasonably understandable geometrical object.

3.1.6 Geometrical requirements of the nets. Topology is invariant to bending, squeezing and twisting as long as no bonds are broken. Many nets can be adjusted so that the dihedral angles between nodes more or less match what is needed between two tris-oxalate complexes. A detailed analysis of some of these geometries is found in ref. 15. Here, in Table 2, we note the ideal densities (as the number of vertices per unit volume) of these nets.

From this point of view it can be noted that the **srs**-net has a very good fit to the oxalate networks, (see ref. 13 and 15 for details) and counter ions like $[M(1,10\text{-bipyridine})_3]^{n+}$ fit nicely inside. It is therefore not surprising that nets with similar densities like **nod** and **lig** form with cations of similar size.

3.1.7 Rationale for topology choice of the system. In the studies surveyed, there has been no single reason pointed out responsible for which network topology any system will adopt. Unfortunately, we cannot point out a single factor either. The following discussion is a summary and a few comments on the rationales given in each individual paper.

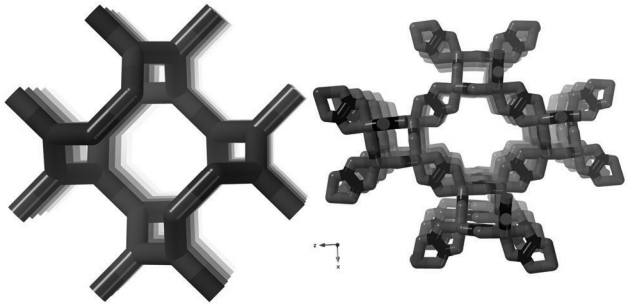

Fig. 2 Left: The ideal **lig**-net. Right: The metal-oxalate network in BEWVEG, $[Mn((S)\text{-salmen})(CH_3OH)_2][MnCr(ox)_3](CH_2Cl_2)_{0.375}(CH_3OH)_{0.375}(H_2O)_{0.125}$, forming the **lig**-net. Note the opposite chirality of the helices (coloured blue and red, left).

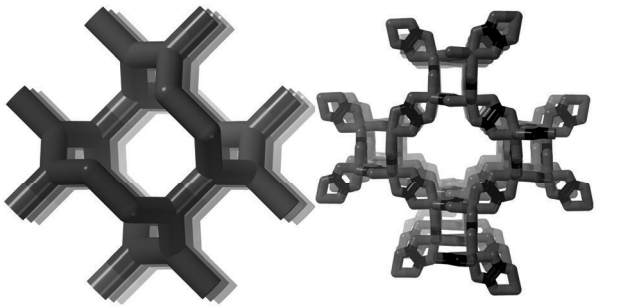

Fig. 3 Left: The ideal **nod**-net. Right: The metal-oxalate network in GURPIT, $[Fe(sal_2\text{-trien})][MnCr(ox)_3]\cdot CH_3OH$, forming the **nod**-net. Note the opposite chirality of the helices (coloured blue and red, left).

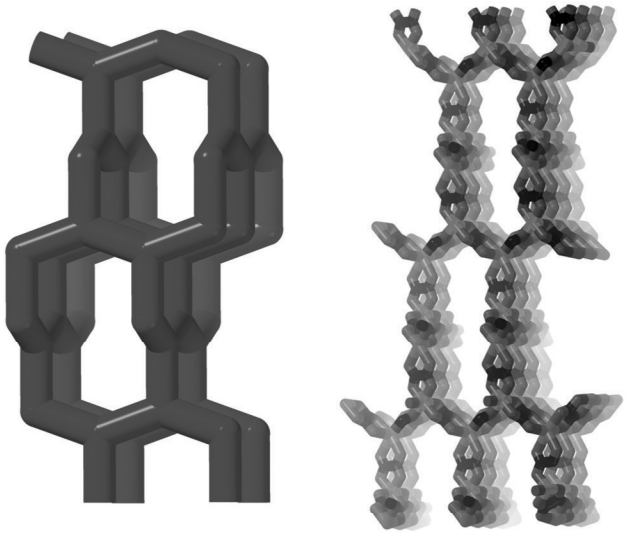

Fig. 4 Left: The ideal **ths**-net. Right: The metal-oxalate network in QIYXIF, [Cu(trans[14]dien)][KCr(ox)$_3$] forming the achiral **ths**-net.

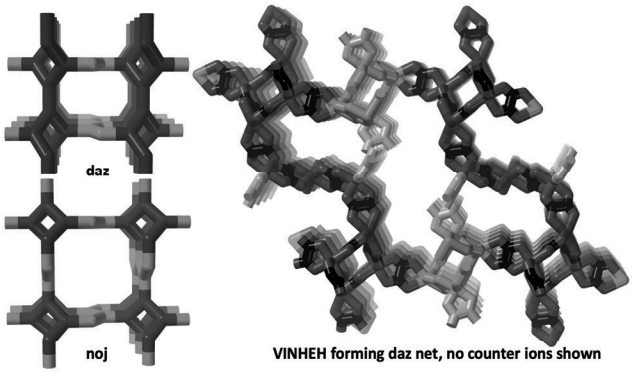

Fig. 6 Left: The ideal tri-nodal **daz**-net and the related **noj**-net. Chirality colour coded as before, in green colour are the non-chiral zigzag connectors. Right: The metal-oxalate network in VINHEH, [Fe(tren(imid)$_3$)]$_2$-[MnCr(ox)$_3$], forming the **daz**-net. Terminating oxalates colour coded yellow and the helices corresponding to the zigzag connection in green just as in the ideal net (left). The **noj**-net is found in XEHXOX.

For clarity, Lewis structures and space filling models of the individual cations are presented in Fig. S2.†

BEWVEG and BEWVOQ are typical examples. The authors demonstrated that using the same cation, [Mn(*R*)-salmen]$^+$ or [Mn(*S*)-salmen]$^+$, the 3D oxalate network depends on the choice of solvent.[28] When crystallized in acetonitrile, a 2D **hcb**-net resulted (BEWVIK and BEWVUW) instead of the 3D **lig**-net obtained from dichloromethane. Pertinent differences between the two structures are the configuration of the two phenoxy arms and the presence of different solvent molecules coordinated to Mn^{III} in the two apical positions of the structure, [Mn(*R*/*S*)-salmen(CH$_3$OH)$_2$]$^+$ for **lig**, whereas the **hcb** ones contain [Mn(*R*/*S*)-salmen(CH$_3$CN)$_2$]$^+$ together with [Mn(*R*/*S*)-salmen(CH$_3$OH)$_2$]$^+$.

VINHOR and VINHIL[33] on the other hand, both **lig**-nets, get their network from the heptacoordinated Mn^{II} ions in each structure. The difference between these structures is that in VINHOR all the Mn atoms are heptacoordinated, and in VINHIL the second crystallographically independent Mn atom is hexacoordinated with a strong trigonal distortion of its octahedral coordination, which give rise to the presence of O–Mn–O angles of 154.6° instead of 180° expected for an octahedral coordination. The methanol in these two complexes is attached to the trioxalate network. Another remark on these two compounds is that the smaller number of cations necessary (+2 *vs.* +1 in *i.e.* BEWVEG) to compensate the negative charge of the oxalate network produces a more irregular network with heptacoordinated Mn^{II} ions coordinated to solvent molecules, and a more open structure with pores filled with disordered solvent molecules.

The **nod**-net in EDATOT[34] may be related to a solvent effect. There is a presence of many interstitial solvent molecules since only one Fe complex is present per Mn/Cr pair, and results in no extra anions needed to stabilize the complex. The lower occupancy of cations and anions inside the anionic network could be the main cause for losing the enantiopure character of these systems.

Combining [Fe^{III}(5-Xsal$_2$-trien)]$^+$ (X = NO$_2$ or CH$_3$O) with the Mn^{II}Cr^{III} oxalates resulted in two different networks.[35] The cation [Fe^{III}(5-NO$_2$sal$_2$-trien)] gave a 2D **hcb**-net (PUWZIZ) since the electron withdrawing group favors π···π stacking interactions between phenyl rings of neighboring cationic complexes. In contrast, in PUWZOX the phenyls are not face to face. This is explained by the presence of the methoxy

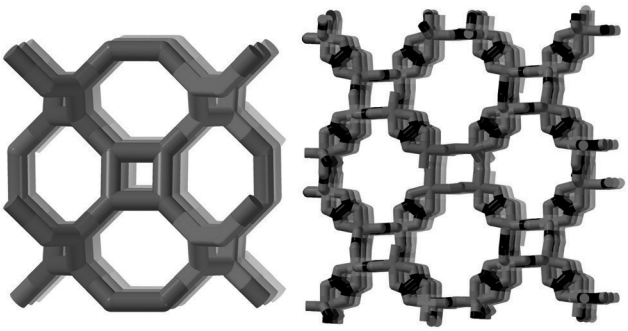

Fig. 5 Left: The ideal **noa**-net. Right: The metal-oxalate network in RUGKIP, (*o*-FAni$^+$)$_2$(DCH[18]crown-6)$_2$[Mn(CH$_3$OH)Cr(oxalate)$_3$][MnCr-(oxalate)$_3$](CH$_3$OH) forming the achiral **noa**-net. The square planar connections are coloured green in both pictures.

Table 2 Densities, as the number of vertices per unit volume, of some selected, ideal, nets. Data from the RCSR

Net	Alt. name	Point symbol	Density[a]
srs	10,3-a	10^3	0.3536
lig	$8^2$10-a	$8^2{\cdot}10$; $8^2{\cdot}10$	0.3536
nod	$8^2$10-b	$8^2{\cdot}10$; $8^2{\cdot}10$	0.3535
bto	10,3-c	10^3	0.5132
ths	10,3-b	10^3	0.4218
utp	10,3-d	10^3	0.4218
noj	8,3-d	8^3; 8^3	0.3241

[a] Number of vertices per unit volume.

groups that hinders the face to face orientation of the neighboring rings. The dihedral angles, α, between the least-squares planes of the two phenoxy rings of the **hcb**-net are α = 89.002° ([Fe1] complex) and α = 94.248° ([Fe2] complex) and the dihedral angles, α, between the phenoxy rings in PUWZOX forming the **nod**-net are for [Fe1A], [Fe1B] and [Fe2] 110.47, 100.41 and 105.55°, respectively. The dihedral angles, α, between the least-squares planes of the two phenoxy rings have very different values in the 2D or 3D structures. Thus, the two phenoxy rings in the 2D compound (PUWZIZ) are closer to 90°, the ideal value for an octahedral complex.

3.1.8 The absence of interpenetration for these systems. The intergrowth of two or more networks is a common feature for coordination polymers,[12,13] and for the **srs**-net in particular many examples exist, see for instance ref. 41. However, in the tris-oxalate systems the **srs**-net is always negatively charged and two such nets interpenetrated in the same compound would require doubling the number of cations while at the same time leaving much less space for them. We believe that these two requirements are difficult to fulfil and therefore interpenetration is not observed in this class of compounds.

3.2 Naturally occurring metal oxalates

Metal oxalates from minerals come in a large variety, from the class of tris-oxalates we have seen in the preceding section, to more or less discrete molecular entities held together by hydrogen bonds. While the former are normally straightforward to analyse, hydrogen bonded systems may be more ambiguous, and even simple metal oxalates may use multiple bonding sites on the oxalates, making some of these systems equally challenging.[36]

In Table 3, we have assembled naturally occurring oxalates according to Piro and Baran[17] with the network analysis performed by our group. We have mainly concentrated on the 3D and 2D coordination polymers, but the very simple humboldtine and lindbergite, the Fe and Mn versions of two isostructural 1D $[M(C_2O_4)(H_2O)_2]$ oxalates, have also been included. In this latter case, the coordination network is supplemented with strong hydrogen bonds between coordinated water and oxalate ions.

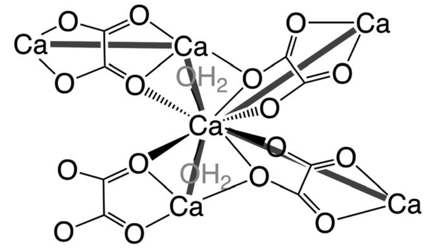

Fig. 7 Weddellite, $[Ca(C_2O_4)(H_2O)_2]\cdot xH_2O$, with a square antiprismatic calcium ion coordinating three oxalate ions and two water molecules forms a four-connected network as indicated by the blue-grey bold lines.

3.2.1 Stepanovite and zhemchuzhnikovite. While stepanovite (OKUTUL03) $[Mg(H_2O)_6][FeNa(C_2O_4)_3]\cdot 3H_2O$ and zhemchuzhnikovite (OKUVAT02) $[Mg(H_2O)_6][AlNa(C_2O_4)_3]\cdot 2H_2O$ form the 2D **hcb**-net in very attractive structures, the hydrated metal ions ($[Mg(H_2O)_6]^{2+}$) that completely fill the voids indicate that these are not real MOFs. The IUPAC definition states that a MOF should be "potentially porous",[25] and as the cations fill the perceived channels, it does not fit the bill. Nevertheless, forming a network of metal carboxylates does make them MOF-like in some aspects.

3.2.2 Weddellite. Weddellite (also "weddelite"), on the other hand, has been reported to lose water without a change in morphology[37] and is thus a potential candidate for a "natural" MOF. This compound, with a square antiprismatic calcium ion coordinating three oxalate ions and two water molecules, has the approximate formula $[Ca(ox)(H_2O)_2]\cdot xH_2O$ and the oxalates bridge the Ca^{2+} ions as depicted in Fig. 7.

The crystal structure according to Tazzoli and Domeneghetti[38] (CSD code WHWLTB) is shown in Fig. 8 together with the **crb**-net formed.

Table 3 Naturally occurring metal-oxalates according to Piro and Baran, and their networks

Compound	Formula	Net	Node[a]
3D coordination networks			
Weddellite	$[Ca(C_2O_4)(H_2O)_2]\cdot xH_2O$	**crb**	Ca
Natroxalate	$[Na_2(C_2O_4)]$	**fit**	Na, ox
Wheatleyite	$[Na_2[Cu(C_2O_4)_2](H_2O)_2]$	**sxd**	Na
Whewellite	$[Ca(C_2O_4)H_2O]$	**sqp**	Ca
Novgorodavaite	$[Ca_2Cl_2(C_2O_4)(H_2O)_2]$	**sqp**	Ca
2D coordination networks			
Zhemchuzhnikovite	$[Mg(H_2O)_6][AlNa(C_2O_4)_3]\cdot 2H_2O$	**hcb**	Mg, Al
Stepanovite	$[Mg(H_2O)_6][FeNa(C_2O_4)_3]\cdot 3H_2O$	**hcb**	Mg, Fe
Deveroite	$[Ce_2(C_2O_4)_3(H_2O)_6]\cdot 4H_2O$	**hcb**	Ce
Coskrenite	$[Ce_2(C_2O_4)(SO_4)_2(H_2O)_8]$	**hxl**	Ce
1D coordination networks or polymers			
Humboldtine	$[Fe(C_2O_4)(H_2O)_2]$	**hum**[b]	Fe, H_2O
Lindbergite	$[Mn(C_2O_4)(H_2O)_2]$	**hum**[b]	Mn, H_2O
Levinsonite	$[Al(H_2O)_6][Y(C_2O_4)(SO_4)_2(H_2O)_3]\cdot 3H_2O$		—
Zugshunstite	$[Al(H_2O)_6][Ce(C_2O_4)(SO_4)_2(H_2O)_3]\cdot 3H_2O$		—

[a] ox = oxalate centroid. [b] New topology.

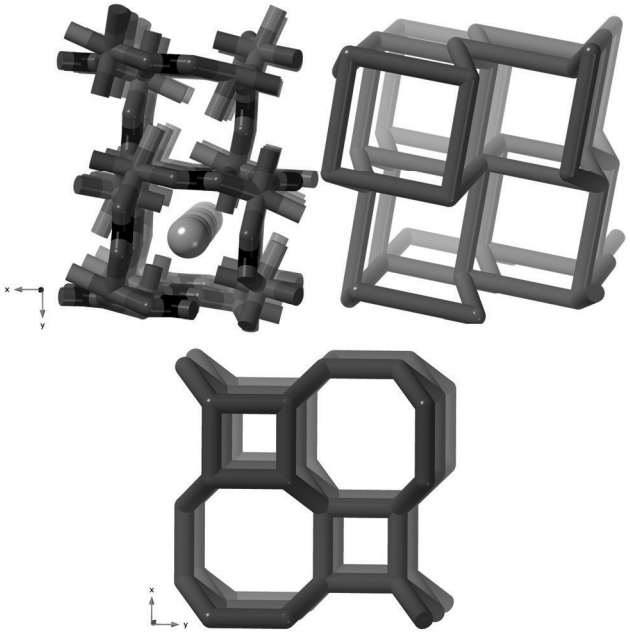

Fig. 8 Top left: Crystal structure of weddellite, $[Ca(C_2O_4)(H_2O)_2]\cdot xH_2O$, water in pink. Top right: The **crb**-net formed. This is the only known naturally occurring metal–organic framework. Bottom: The ideal **crb**-net.

The porosity of weddellite has not been rigorously proven. However, in a study using an environmental scanning electron microscope with a heating stage attached, no changes in the crystal morphology were observed as water was desorbed[37] and recently detailed variable temperature single crystal and powder X-ray diffraction (XRD) has confirmed structural integrity up to 105–140 °C after which the structure collapses.[39]

3.2.3 Natroxalate. In the crystal structure of natroxalate, $[Na_2(C_2O_4)]$ (CSD code NAOXAL – NAOXAL20), we no longer see distinct oxalate bridges, but rather a much more tightly packed system. In this compound every sodium ion binds to five oxalate ions, and every oxalate to ten sodium ions. The analysis is very straightforward, generating the 5 and 10 connected **fit**-net shown in Fig. 9.

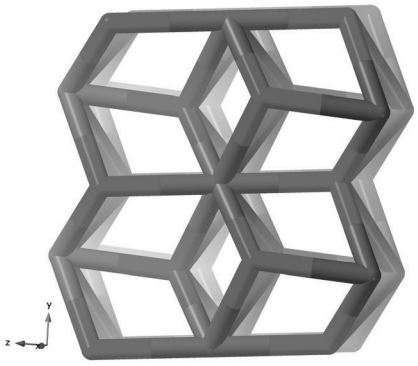

Fig. 9 The 5 (Na^+, pink) and 10 (oxalate centroids, green) connected **fit**-net in natroxalate, $[Na_2(C_2O_4)]$. This is a tightly packed structure without voids.

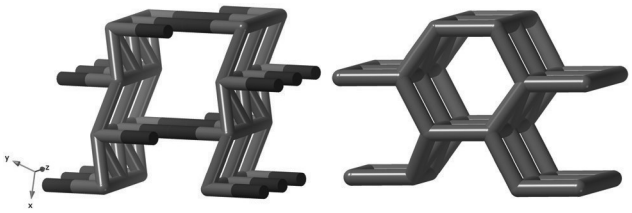

Fig. 10 Left: The **sxd**-net in wheatleyite, $[Na_2Cu(C_2O_4)_2]\cdot 2H_2O$, orange is Na^+ and mauve represents the $[Cu(C_2O_4)_2]^{2-}$ bridge. Right: The ideal **sxd**-net.

3.2.4 Wheatleyite. Wheatleyite is a mixed-metal mineral with formula $[Na_2Cu(C_2O_4)_2]\cdot 2H_2O$ (CSD code CUOXNAII) composed of layers of sodium ions doubly bridged by oxygens from either oxalate or water that are connected through the $[Cu(C_2O_4)_2]^{2-}$ bridge.

This forms the six-connected **sxd**-net and the network in the wheatleyite structure is shown in Fig. 10 together with the most symmetric form of the net.

3.2.5 Deveroite. Deveroite, $[Ce_2(C_2O_4)_3(H_2O)_6]\cdot 4H_2O$ CSD code CEOXDH, also forms the 2D **hcb**-net despite Ce^{3+} being 9-coordinated. In contrast to stepanovite and zhemchuzhnikovite there are no counter ions that plug the empty space in the centre of the hexagons. However, the layers pack in an ABAB-fashion, with an offset, so that edges of layer A are in the middle of the hexagonal window of layer B, so no continuous open channels exist in this compound.

3.2.6 Whewellite. In whewellite, $[Ca(C_2O_4)(H_2O)]$ CSD code CALOXM, as in weddellite, we find a square antiprismatic calcium ion with two bis-chelating oxalate ions. One water and oxygen atoms from three other oxalate ions complete the coordination sphere, making every calcium ion a five-connected node in an **sqp**-net, see Fig. 11.

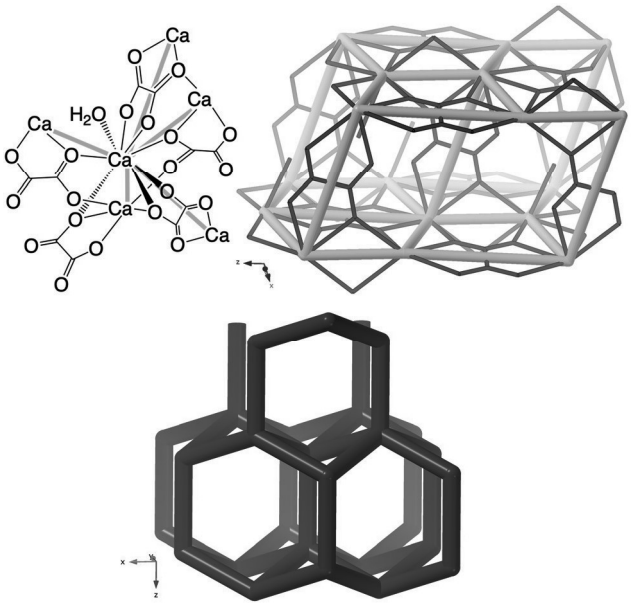

Fig. 11 Top left: Whewellite, $[Ca(C_2O_4)(H_2O)]$, with every Ca^{2+} five-connected node in an **sqp**-net. Top right: The **sqp**-net in whewellite. Below: The ideal **sqp**-net.

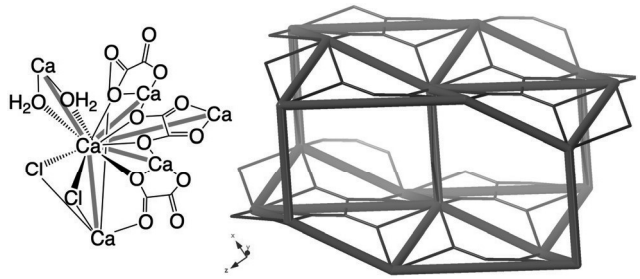

Fig. 12 Top left: Novgorodavaite, $[Ca_2Cl_2(C_2O_4)(H_2O)_2]$, with every Ca^{2+} five-connected node in an **sqp**-net. Top right: The **sqp**-net in novgorodavaite. The ideal **sqp**-net is shown in Fig. 11.

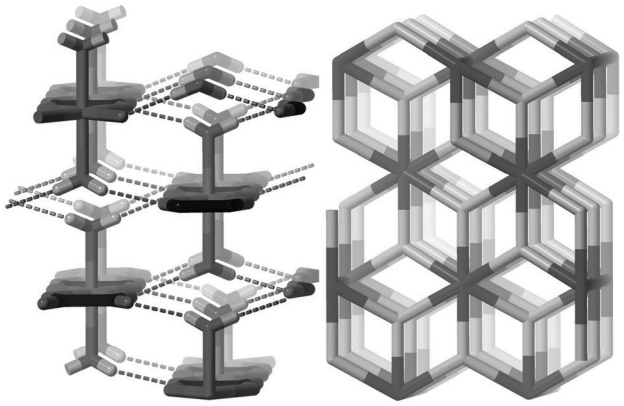

Fig. 13 The new 3- and 8-connected net **hum** (right) is formed from Fe and Mn (8-connect nodes) versions of $[M(C_2O_4)(H_2O)_2]$ *via* 1D coordination polymers and hydrogen bonding between coordinated water (3-connect node) and oxalate (left).

Inspecting this structure, one finds apparent voids, but they are all too small to be chemically significant.

3.2.7 Coskrenite. Coskrenite, $[Ce_2(C_2O_4)(SO_4)_2(H_2O)_8]$, again forms a 2D network, a corrugated version of the six-connected **hxl**-net with lanthanoid ions (many possibilities exist) bridged by oxalates and sulfates. Structure data from entry 9004543 in the Crystallography Open Database.

3.2.8 Novgorodavaite. Novgorodavaite $[Ca_2Cl_2(C_2O_4)(H_2O)_2]$ resembles whewellite in that it also forms a five-connected net with an **sqp** topology, see Fig. 12. Structure data from entry 0012496 in the American Mineralogist Crystal Structure Database.

3.2.9 1D coordination polymers. The 1D coordination polymers are all straight chains with bis-chelating oxalates, M–oxalate–M. They all form hydrogen bonded networks, some more complex than others. Here, we consider only the isostructural humboldtine and lindbergite, the Fe and Mn versions of $[M(C_2O_4)(H_2O)_2]$, respectively.

They have infinite bis-chelating –M–oxalate–M– chains with perpendicular coordinated water molecules, each hydrogen bonding to two oxalates. Taking the metal ions as one node and the water molecules as another, these structures form 3- and 8-connected nets. The water nodes are three-connected as they bind to the metal ion and then hydrogen bonds to two oxalates each. The metal ion node is eight connected as it binds to metal ions through coordination, two water molecules also *via* coordination, and then four waters *via* hydrogen bonds. This new topology **hum** is shown in Fig. 13 (right) together with the structure of humboldtine.

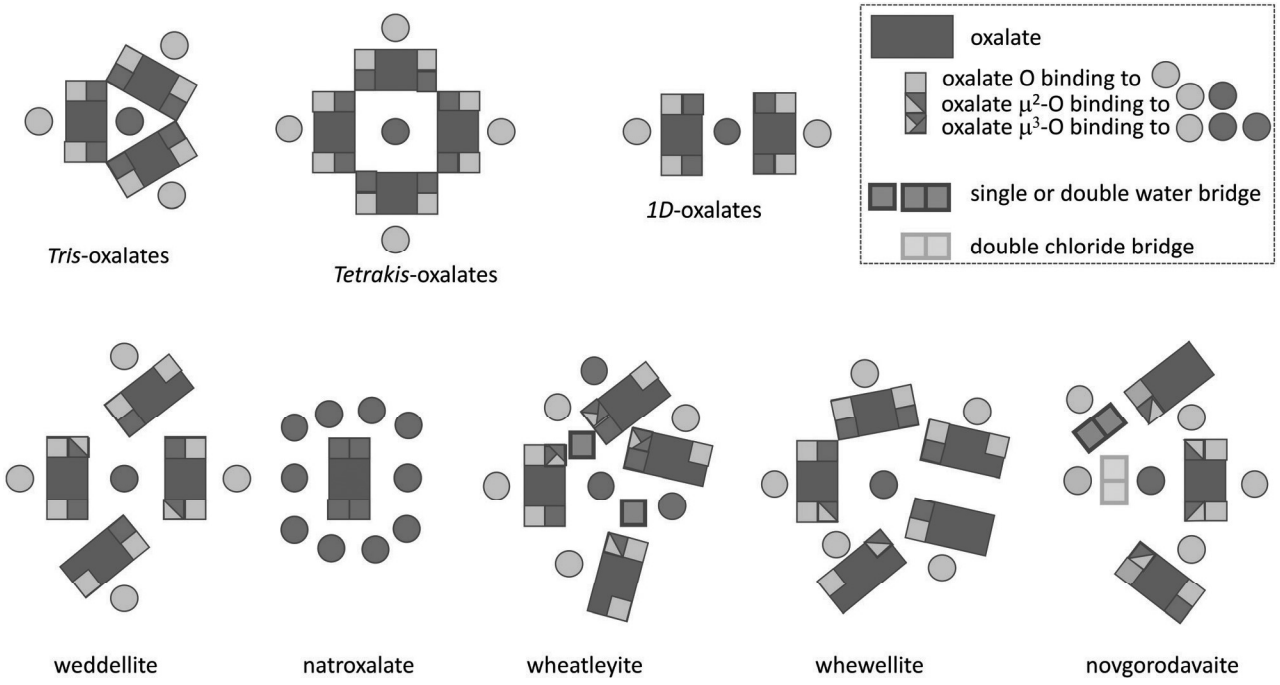

Fig. 14 Schematic overview of the connectivity of the oxalates discussed in this article, including the tetrakis-oxalates only briefly mentioned.

4. Conclusions

Analysis of the CSD data indicates that synthetic 3D tris-oxalates occur in more than one network topology, even if the **srs**-net is by far the most common. The well-known nets **nod**, **lig**, and **ths** were found to occur, together with the new topologies **noa** and **daz**. It also suggests that, as different topologies have differently shaped and sized cavities, a rational approach to design compounds with other network topologies not encountered so far, should be possible.

Even so, the examples provided here give no clear guidance as how to perform such a rational design. Computational studies are in progress to address this question.

We also note that the issue may be more complex than a simple consideration of ideal geometries may suggest. Topologies stay the same even if bent, squeezed or otherwise distorted, as long as no bonds in the network are broken. Thus both the relative size and the shape of the empty space inside a particular network may be changed without changing the topology. Excellent examples are the "breathing" MOFs such as MIL-53.[40] Indeed we suggest that it should be possible to calculate a figure of merit for each network topology on the relative energetic cost of different distortions to further enhance their utility as blueprints for the design of molecule based materials.

We also note that the synthetic tris-oxalates are often multi component systems where the network can interplay with one or more guests.[41] Taking the network topology into consideration will be one important step in making the synthesis of such materials a more rational process.

The natural oxalates present a more complex picture, and in Fig. 14 we have tried to summarize and contrast them to the more symmetric synthetic analogues. The new net **hum** was described as a model for the bonding and structure in humboldtine and lindbergite.

Conflicts of interest

There are no conflicts to declare.

Acknowledgements

CLFD, FMAN, and LÖ thank the Swedish Research Council. We are grateful to Prof. Michael O'Keeffe for adding the new network topologies **noa**, **mys**, **daz** and **hum** to the RCSR database.

Notes and references

1 L. Öhrström and J. Covès, *The Rhubarb Connection and Other Revelations: The Everyday World of Metal Ions*, Royal Society of Chemistry, London, 2018.
2 I. Huskić, N. Novendra, D.-W. Lim, F. Topić, H. M. Titi, I. V. Pekov, S. V. Krivovichev, A. Navrotsky, H. Kitagawa and T. Friščić, *Chem. Sci.*, 2019, **10**, 4923–4929.
3 F. Y. Yi, H. J. Yang, X. Zhao, P. Y. Feng and X. H. Bu, *Angew. Chem., Int. Ed.*, 2019, **58**, 2889–2892.
4 B. Zhang, P. J. Baker, Y. Zhang, D. Wang, Z. Wang, S. Su, D. Zhu and F. L. Pratt, *J. Am. Chem. Soc.*, 2018, **140**, 122–125.
5 M. Darawsheh, L. A. Barrios, O. Roubeau, S. J. Teat and G. Aromí, *Angew. Chem., Int. Ed.*, 2018, **57**, 13509–13513.
6 P. K. Tsobnang, E. Hastürk, D. Fröhlich, E. Wenger, P. Durand, J. L. Ngolui, C. Lecomte and C. Janiak, *Cryst. Growth Des.*, 2019, **19**, 2869–2880.
7 C. F. N. Nguemdzi, F. Capet, J. Ngouné, G. Bebga, M. Foulon and J. Nenwa, *J. Coord. Chem.*, 2018, **71**, 1484–1496.
8 G. W. Burgers and W. Bragg, *Proc. R. Soc. London, Ser. A*, 1927, **116**, 553–586.
9 A. F. Wells, *Three-dimensional nets and polyhedra*, John Wiley & Sons, New York, 1977.
10 A. F. Wells, *Acta Cryst.*, 1954, **7**, 535–544.
11 O. M. Yaghi, M. O'Keeffe, N. W. Ockwig, H. K. Chae, M. Eddaoudi and J. Kim, *Nature*, 2003, **423**, 705–714.
12 V. A. Blatov, L. Carlucci, G. Giani and D. M. Proserpio, *CrystEngComm*, 2004, **6**, 377–395.
13 L. Öhrström and K. Larsson, *Molecule-Based Materials The Structural Network Approach*, Elsevier, Amsterdam, 2005.
14 L. Öhrström, *Chem. – Eur. J.*, 2016, **22**, 13758–13763.
15 L. Öhrström and K. Larsson, *Dalton Trans.*, 2004, 347–353.
16 L. Öhrström and K. Larsson, *Molecule-Based Materials: The Structural Network Approach*, Elsevier, Amsterdam, 2005, ch. 12.
17 O. E. Piro and E. J. Baran, *Crystallogr. Rev.*, 2018, **24**, 149–175.
18 I. Huskic and T. Friscic, *Acta Crystallogr., Sect. B: Struct. Sci., Cryst. Eng. Mater.*, 2018, **74**, 539–559.
19 B. Smith, *'Designer' materials found deep in Siberian permafrost*, Cosmos, 2016, 08 AUGUST.
20 E. Stoye, Naturally occurring MOFs found in coal mine minerals, *Chemistry World*, RSC, 2016, 19 AUGUST.
21 I. Huskic, I. V. Pekov, S. V. Krivovichev and T. Friscic, *Sci. Adv.*, 2016, **2**, 7.
22 V. A. Blatov, A. P. Shevchenko and D. M. Proserpio, *Cryst. Growth Des.*, 2014, **14**, 3576–3586.
23 O. Delgado-Friedrichs and M. O'Keeffe, *Acta Crystallogr., Sect. A: Found. Crystallogr.*, 2003, **59**, 351–360.
24 M. O'Keeffe, M. A. Peskov, S. Ramsden and O. M. Yaghi, *Acc. Chem. Res.*, 2008, **41**, 1782–1789.
25 S. R. Batten, N. R. Champness, X. M. Chen, J. Garcia-Martinez, S. Kitagawa, L. Öhrström, M. O'Keeffe, M. P. Suh and J. Reedijk, *Pure Appl. Chem.*, 2013, **85**, 1715–1724.
26 A. Mizuno, Y. Shuku and K. Awaga, *Bull. Chem. Soc. Jpn.*, 2019, **92**, 1068–1093.
27 N. L. Rosi, J. Kim, M. Eddaoudi, B. Chen, M. O'Keeffe and O. M. Yaghi, *J. Am. Chem. Soc.*, 2005, **127**, 1504–1518.
28 M. Clemente-León, E. Coronado and M. López-Jordà, *Dalton Trans.*, 2013, **42**, 5100–5110.
29 V. A. Blatov, M. O'Keeffe and D. M. Proserpio, *CrystEngComm*, 2010, **12**, 44–48.
30 M. Clemente-León, E. Coronado, M. López-Jordà, G. Mínguez Espallargas, A. Soriano-Portillo and J. C. Waerenborgh, *Chem. – Eur. J.*, 2010, **16**, 2207–2219.
31 H.-Y. Shen, W.-M. Bu, D.-Z. Liao, Z.-H. Jiang, S.-P. Yan and G.-L. Wang, *Inorg. Chem.*, 2000, **39**, 2239–2242.

32 T. Endo, K. Kubo, M. Yoshitake, S.-i. Noro, N. Hoshino, T. Akutagawa and T. Nakamura, *Cryst. Growth Des.*, 2015, **15**, 1186–1193.
33 A. Ben Djamâa, M. Clemente-León, E. Coronado and M. López-Jordà, *Polyhedron*, 2013, **64**, 142–150.
34 E. Coronado, J. R. Galán Mascarós, M. C. Giménez-López, M. Almeida and J. C. Waerenborgh, *Polyhedron*, 2007, **26**, 1838–1844.
35 M. Clemente-León, E. Coronado and M. López-Jordà, *Dalton Trans.*, 2010, **39**, 4903–4910.
36 C. Borel, M. Ghazzali, V. Langer and L. Öhrström, *Inorg. Chem. Commun.*, 2009, **12**, 105–108.
37 J. T. Kloprogge, T. E. Bostrom and M. L. Weier, *Am. Mineral.*, 2004, **89**, 245–248.
38 V. Tazzoli and C. Domeneghetti, *Am. Mineral.*, 1980, **65**, 327–334.
39 A. R. Izatulina, V. V. Gurzhiy, M. G. Krzhizhanovskaya, M. A. Kuz'mina, M. Leoni and O. V. Frank-Kamenetskaya, *Cryst. Growth Des.*, 2018, **18**, 5465–5478.
40 L. R. Parent, C. H. Pham, J. P. Patterson, M. S. Denny, S. M. Cohen, N. C. Gianneschi and F. Paesani, *J. Am. Chem. Soc.*, 2017, **139**, 13973–13976.
41 M. Ghazzali, V. Langer, K. Larsson and L. Öhrström, *CrystEngComm*, 2011, **13**, 5813–5817.